Appl. Phys. B (2014) 117:621–631
DOI 10.1007/s00340-014-5875-1

Applied Physics B
Lasers and Optics

Energy extraction in dual-wavelength Q-switched laser with a common upper laser level

Atsushi Sato · Shimpei Okubo · Kazuhiro Asai · Shoken Ishii · Kohei Mizutani

Received: 20 September 2013 / Accepted: 4 June 2014 / Published online: 15 June 2014

Abstract The effect of lower-laser-level lifetimes on Q-switched pulse generation in a dual-wavelength solid-state laser with a common upper laser level was numerically and experimentally investigated. A rate-equation model that accounts for finite lower-laser-level lifetimes was developed, and for a Nd:YAG laser operating at 1064 and 1319 nm, numerical simulations of dual-wavelength pulse generation were performed with and without the effects of lower-laser-level lifetimes. In the laser experiments, characteristics of the dual-wavelength Q-switched pulses agree reasonably well with theoretical predictions. As a result, we found that both the total energy of the two Q-switched pulses and the ratio of 1064–1319-nm pulse energies were strongly affected by the lower-laser-level lifetimes when the Q-switched pulse width was comparable or shorter than the lower-laser-level lifetime.

1 Introduction

Dual-wavelength Q-switched lasers are useful for differential absorption measurements, imaging, spectroscopy, and medical applications because the fundamental waves and their nonlinear frequency conversion can cover a vast spectral range from visible to terahertz (THz) [1–4]. A dual-wavelength laser with a single pump laser head offers several advantages such as cost effectiveness, compactness, and a coaxial output of two laser beams due to a shared output mirror. Moreover, dual-wavelength lasing using a common upper laser level with the longest lifetime provides a simple pumping scheme and high-energy storage capability in Q-switched operations. In most of these lasers, the stimulated-emission cross sections of the two wavelengths are different [1, 2]. Therefore, to compensate for the difference in the stimulated-emission cross section between the two laser transitions, the output coupling and cavity length of the laser operating at the higher-gain emission line must be made larger and longer, respectively, than those for the lower-gain emission line [2, 5–7]. However, such cavity designs often differ from optimum conditions for single-emission-line operation, and in particular, they tend to increase the pump threshold when operating the laser at the higher-gain emission line. Additionally, fluctuations in laser output become significantly large using this method because line competition occurs between the two emission lines [8–10]. However, intermittent oscillation of dual-wavelength lasers permits stable operation without line competition under optimum cavity designs. Earlier, it was difficult to obtain temporal overlap between two pulses because the time interval between the first and second pulse was of the order of tens of microseconds as a result of the pumping required for the second pulse [11]. Further investigations of the intermittent oscillation using a passively Q-switched Nd:YVO_4 laser was reported by Huang et al. and Xu et al. [12, 13]. They demonstrated simultaneous dual-wavelength Q-switched operation and pointed out the contribution to the second pulse of the residual population inversion that remains after extracting the first pulse. However, when the pulse width in Q-switched lasers is comparable or shorter than the lower-laser-level lifetime, which is of the order of several tens of

A. Sato (✉) · S. Okubo · K. Asai
Tohoku Institute of Technology, 35-1 Yagiyama-Kasumi-cho, Taihaku-ku, Sendai 982-8577, Japan
e-mail: atsushi@tohtech.ac.jp

S. Ishii · K. Mizutani
National Institute of Information and Communications Technology, 4-2-1 Nukui-Kitamachi, Koganei-shi, Tokyo 184-8795, Japan

nanoseconds in the case of Nd-doped lasers [14], the laser performance is affected by the population in the lower laser level during Q-switched pulse evolution [15]. In dual-wavelength Q-switched lasers that use the residual population inversion left after energy extraction by the first pulse (i.e., the two-step energy extraction technique), this effect cannot be neglected because the final population density for the first pulse is not equal to the initial population-inversion density for the second pulse because of the difference in population density between the two lower laser levels. Nevertheless, theoretical analysis that accounts for the finite lower-laser-level lifetimes in dual-wavelength Q-switched lasers has not yet been reported.

We investigate the effects of lower-laser-level lifetimes on Q-switched pulse generation in a dual-wavelength solid-state laser with a common upper laser level. A rate-equation model that accounts for finite lower-laser-level lifetimes is developed, and numerical simulations are reported to investigate the behavior of a dual-wavelength Q-switched laser operating with (1) simultaneous and (2) two-step energy extraction. Additionally, experimental results obtained with an actively Q-switched Nd:YAG laser operating at 1064 and 1319 nm are compared with the theoretical predictions.

2 Theoretical analysis

Figure 1 shows the energy-level diagram for Nd in YAG. The lasing wavelengths of interest in this study are 1064 and 1319 nm, which correspond to the $^4F_{3/2} \rightarrow {}^4I_{11/2}$ and $^4F_{3/2} \rightarrow {}^4I_{13/2}$ transitions, respectively. While the upper laser manifold $^4F_{3/2}$ consists of two Stark levels, only the R_2 level is used as a common upper laser level for both transitions. The 1064- and 1319-nm transitions terminate on the Y_3 and X_1 levels, respectively. Rate-equation models for a dual-wavelength Q-switched laser with a common upper laser level have been developed in previous studies [5, 16, 17]. These models assumed that the population-inversion density is given by the population density in the upper laser level. If the lower-laser-level lifetime was significantly shorter than the Q-switched pulse width, this assumption is reasonable because the population of the lower laser level is negligible because the relaxation of ions from the lower laser level to the ground state occurs in a time much shorter than the pulse width. However, this assumption is invalid if the lower-laser-level lifetime is comparable to or longer than the Q-switched pulse width. In this case, the population of the lower laser level is nonzero during pulse evolution and is therefore depleted by the pulse, which decreases the population inversion. For example, when the first and second Q-switched pulses are extracted in succession after one pumping cycle (i.e., two-step energy extraction), the initial and threshold population-inversion densities for the first Q-switched pulse significantly influence the residual population, which corresponds to the initial population for the second Q-switched pulse. Therefore, population densities and lifetimes in the two lower laser levels must be accounted for in the model.

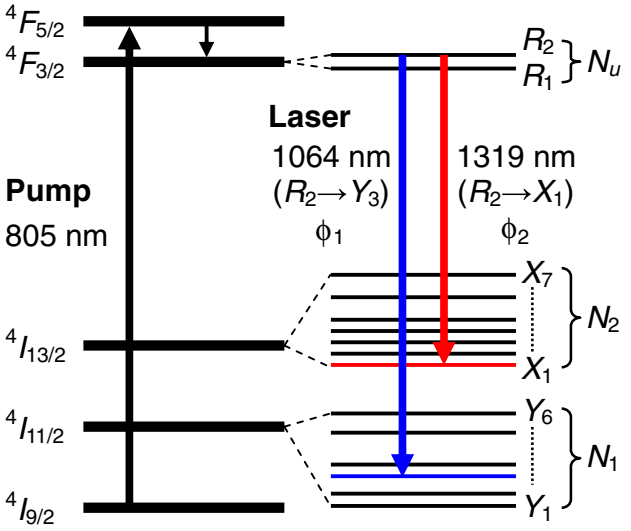

Fig. 1 Energy level diagram for Nd:YAG

Equations (1)–(5) represent the coupled rate equations for this model:

$$\frac{dN_u}{dt} = W_p - \frac{N_u}{\tau_f} - \frac{c}{n_r}\sigma_1\varphi_1(f_u N_u - f_1 N_1) - \frac{c}{n_r}\sigma_2\varphi_2(f_u N_u - f_2 N_2), \quad (1)$$

$$\frac{dN_2}{dt} = \frac{\beta_2 N_u}{\tau_f} + \frac{c}{n_r}\sigma_2\varphi_2(f_u N_u - f_2 N_2) - \frac{N_2}{\tau_2}, \quad (2)$$

$$\frac{dN_1}{dt} = \frac{\beta_1 N_u}{\tau_f} + \frac{c}{n_r}\sigma_1\varphi_1(f_u N_u - f_1 N_1) - \frac{N_1}{\tau_1}, \quad (3)$$

$$\frac{d\varphi_2}{dt} = \frac{cl}{n_r l_{c2}}\sigma_2\varphi_2(f_u N_u - f_2 N_2) - \frac{\varphi_2}{\tau_{c2}} + \frac{\gamma_2\beta_2 N_u}{\tau_f}, \quad (4)$$

$$\frac{d\varphi_1}{dt} = \frac{cl}{n_r l_{c1}}\sigma_1\varphi_1(f_u N_u - f_1 N_1) - \frac{\varphi_1}{\tau_{c1}} + \frac{\gamma_1\beta_1 N_u}{\tau_f}, \quad (5)$$

where N_u, (N_1 and N_2) is (are) the population densities in the upper (lower) laser manifolds, ϕ_1 and ϕ_2 are the laser photon densities in the laser cavities, W_p is the pumping rate, τ_f is the lifetime of the upper laser manifold, τ_1 and τ_2 are the lifetimes of the lower laser manifold, σ_1 and σ_2 are the stimulated-emission cross sections for two transitions, c is the speed of light in vacuum, n_r is the refractive index of the laser medium, f_u (f_1 and f_2) is (are) the Boltzmann thermal occupation factors of the upper (lower) laser levels,

τ_{c1} and τ_{c2} are the photon decay times in the laser cavities, l is the length of the laser rod, l_{c1} and l_{c2} are the effective lengths of the cavities, γ_1 and γ_2 are the rates at which spontaneous emission contributes to the lasers, and β_1 and β_2 are the branching ratios. The subscripts 1 and 2 in the equations correspond to the laser transitions at 1064 and 1319 nm, respectively. We assumed a conventional Y-shaped cavity [18] that was used in our experiments (described in a later section). In this configuration, an output mirror and a laser pump head are shared between two lasers, and a Q-switch and a rear mirror for each laser are placed in the respective arms of the laser cavity. The photon decay times in the laser cavities are given by

$$\tau_{c1} = -\frac{2l_{c1}}{c\ln[(1-L_{c1})(1-L_{Q1})R_1]}, \tag{6}$$

$$\tau_{c2} = -\frac{2l_{c2}}{c\ln[(1-L_{c2})(1-L_{Q2})R_2]}, \tag{7}$$

where L_{c1} and L_{c2} are the roundtrip losses in the laser cavities, R_1 and R_2 are the reflectivities of the output mirrors, and L_{Q1} and L_{Q2} are the time-dependent losses introduced by the Q-switches. The Q-switch losses can be approximated by

$$L_{Q1} = \begin{Bmatrix} L_{max1} & (0 < t \le t_{Q1}) \\ 0 & (t_{Q1} < t) \end{Bmatrix}, \tag{8}$$

$$L_{Q2} = \begin{Bmatrix} L_{max2} & (0 < t \le t_{Q2}) \\ 0 & (t_{Q2} < t) \end{Bmatrix}, \tag{9}$$

where L_{max1} and L_{max2} are the maximum Q-switch losses and t_{Q1} and t_{Q2} are the delay times of the Q-switches with respect to the beginning of the pump pulse.

This model was used to simulate Q-switched pulses in a dual-wavelength Nd:YAG laser operating at 1064 and 1319 nm. The parameters used in the simulation are given in Table 1. The pump pulse is shorter than the conventional pulse width of 230 μs because of the limitation due to amplified spontaneous emission (described in a later section). The quantities γ_1 and γ_2 are obtained by accounting for the spontaneous emission within a solid angle at the cavity mirrors. A rough estimate of γ_1 and γ_2 is acceptable because the last terms in (4) and (5) affect only the temporal Q-switched pulse position. Published values of the lifetime τ_1 of the lower laser manifold $^4I_{11/2}$ vary widely. Hovis et al. observed an upper limit of 11 ns for the $^4I_{11/2}$ manifold lifetime by measuring the time-dependent gain of a Q-switched Nd:YAG laser [19]. Bibeau et al. measured the $^4I_{11/2}$ manifold lifetime using the energy gap law and reported a significantly short value of 115–225 ps [20]. Degnan et al. performed the numerical simulations of a Q-switched Nd:YAG laser using a model that considers thermalization and relaxation; their results were at odds with the subnanosecond lifetime [14]. In our preliminary experiments, a satellite pulse was often observed during several tens of nanoseconds after the main Q-switched pulse. This results from the gain recovery caused by the finite lower laser level lifetime [21]. Previous studies and our results suggest that the $^4I_{11/2}$ manifold lifetime is shorter than several tens of nanoseconds. Therefore, we assume $\tau_1 = 11$ ns in our simulation. On the other hand, an accurate value for the lifetime τ_2 of the lower laser manifold $^4I_{13/2}$ is unknown. We assumed $\tau_2 = 80$ ns in our simulation on the basis of the observations of the satellite pulse as with τ_1.

Table 1 Parameters used in numerical simulations [22, 23]

Description, symbol (unit)	Value
Pump wavelength (nm)	805
Pump pulse length (μs)	140
Stimulated-emission cross section at 1064 nm, σ_1 (10^{-20} cm^2)	45.8
Stimulated-emission cross section at 1319 nm, σ_2 (10^{-20} cm^2)	8.7
Lifetime τ_f of the upper laser manifold (μs)	230
Thermal occupation factor of the upper laser level, f_u	0.40
Thermal occupation factor of the lower laser level for the 1064 nm transition, f_1	0.19
Thermal occupation factor of the lower laser level for the 1319 nm transition, f_2	0.32
Length of the laser rod, l (mm)	10
Diameter of the laser rod (mm)	3
Cavity length for the 1064 nm laser, l_{c1} (mm)	530
Cavity length for the 1319 nm laser, l_{c2} (mm)	650
Refractive index, n_r	1.82
Pumping rate, W_p (10^{22} cm^{-3}s^{-1})	7
Branching ratio for the R_2 to Y_3 levels, β_1	0.135
Branching ratio for the R_2 to X_1 levels, β_2	0.018
Roundtrip loss of the 1064 nm laser cavity, L_{c1}	0.03
Roundtrip loss of the 1319 nm laser cavity, L_{c2}	0.03

Figure 2 shows the results ϕ_1 and ϕ_2 of the numerical simulation with respect to the laser photon densities in the cavities and the population density N_u in the upper laser manifold as a function of time. For convenience, we define a time interval Δt_Q between two Q-switch delay times as $\Delta t_Q = t_{Q1} - t_{Q2}$. The value of Δt_Q is between 180 and 240 ns, and a positive sign for Δt_Q means that the Q-switch for the 1319 nm laser opens before that for the 1064 nm laser. The horizontal axis represents the time after the pump pulse ends. In Figs. 2a–d, the lower-laser-level lifetimes were set to zero so that the population-inversion densities for both transitions were equal to the population-inversion density of the upper laser level. Conversely, Fig. 2e–h show the results when the effects of the lower-

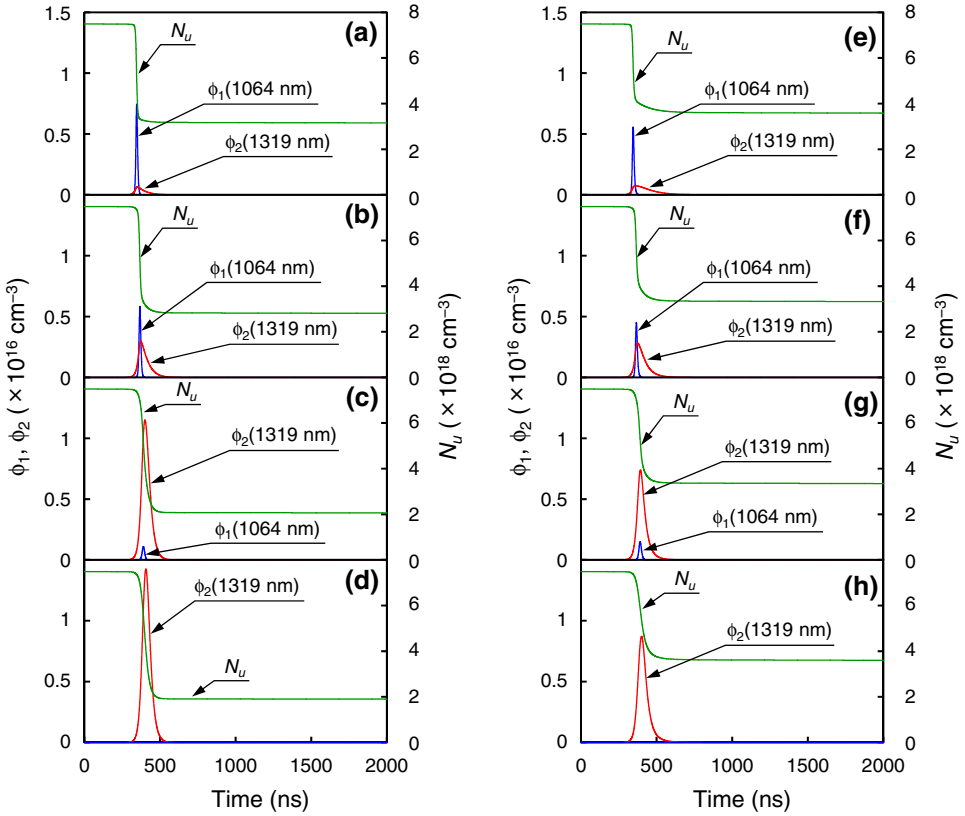

Fig. 2 Results of numerical simulation for dual-wavelength Q-switched operation under simultaneous energy extraction. *Panels* **a**–**d** $\tau_1 = \tau_2 = 0$ ns; *panels* **e**–**h** $\tau_1 = 11$ ns, $\tau_2 = 80$ ns. **a** and **e** $\Delta t_Q = 180$ ns; **b** and **f** $\Delta t_Q = 200$ ns; **c** and **g** $\Delta t_Q = 220$ ns; **d** and **h** $\Delta t_Q = 240$ ns. Reflectivities of the output mirrors for 1064 and 1319 nm lasers are $R_1 = 8$ % and $R_2 = 70$ %, respectively

laser-level lifetimes are accounted for and with the assumptions $\tau_1 = 11$ ns and $\tau_2 = 80$ ns. The output mirror reflectivities for the 1064 and 1319 nm laser lines were set to 8 and 70 %, respectively. In this situation (the dual-wavelength regime), two Q-switched pulses were simultaneously extracted although the pulse widths of the two pulses differ (Fig. 2a–c, e–g). The pulse widths for the 1064 and 1319 nm lasers were 12–14 ns and 54–69 ns, respectively, well above threshold. Since these pulse widths were comparable or shorter than the assumed lower-laser-level lifetimes, effects of the population in the lower laser levels appeared to increase in the residual population of the upper laser manifold after lasing. The reason the residual population density in Fig. 2e–h is higher than those in Fig. 2a–d is that the population in the lower laser level reduces the population-inversion density, thereby reducing the stimulated-emission gain for the same population density of the upper laser level. In the case of the simultaneous energy extraction in dual-wavelength lasing, both Q-switched pulses can be extracted by adjusting the time interval between the two Q-switched pulses despite the residual population of the upper laser level being affected by the lower-laser-level lifetime.

The situation is different for Q-switched pulses extracted by the two-step process: The ratio of the 1064–1319-nm pulse energies can be chosen only by changing the cavity design parameters such as output couplings and cavity losses. Two-step energy extraction has an advantage over the simultaneous energy extraction because it permits stable operation without line competition between the two transitions. Figure 3 shows the results of simulations for two-step energy extraction. The parameters used for these simulations are the same as for Fig. 2 except that the reflectivities of the output mirrors for the 1064 and 1319 nm lasers were set to 30 and 55–70 %, respectively, to obtain a first pulse at 1319 nm and a second pulse at 1064 nm. While the time interval between two Q-switch delay times Δt_Q was roughly chosen to avoid temporal overlap between the two pulses, it is not important because this parameter does not affect pulse shape or intensity. For Fig. 3a, e, the pulse widths of the first pulse are longer than 200 ns, which is over 2.5 times longer than the assumed lower-laser-level lifetime of the 1319-nm transition. In this case, the residual population density of the upper laser manifold increased by a factor of 1.06 due to the effect of the lower-laser-level lifetime. In comparison, when the reflectivity of the output mirror for the 1319 nm laser was 65 %, the pulse width of the first pulse was 72–77 ns, which is slightly shorter than the assumed lower-laser-level lifetime, and the ratio of the residual population densities in Fig. 3g, c increased to 1.48. Furthermore, this ratio increased to 1.91 for the output mirror with 70 %

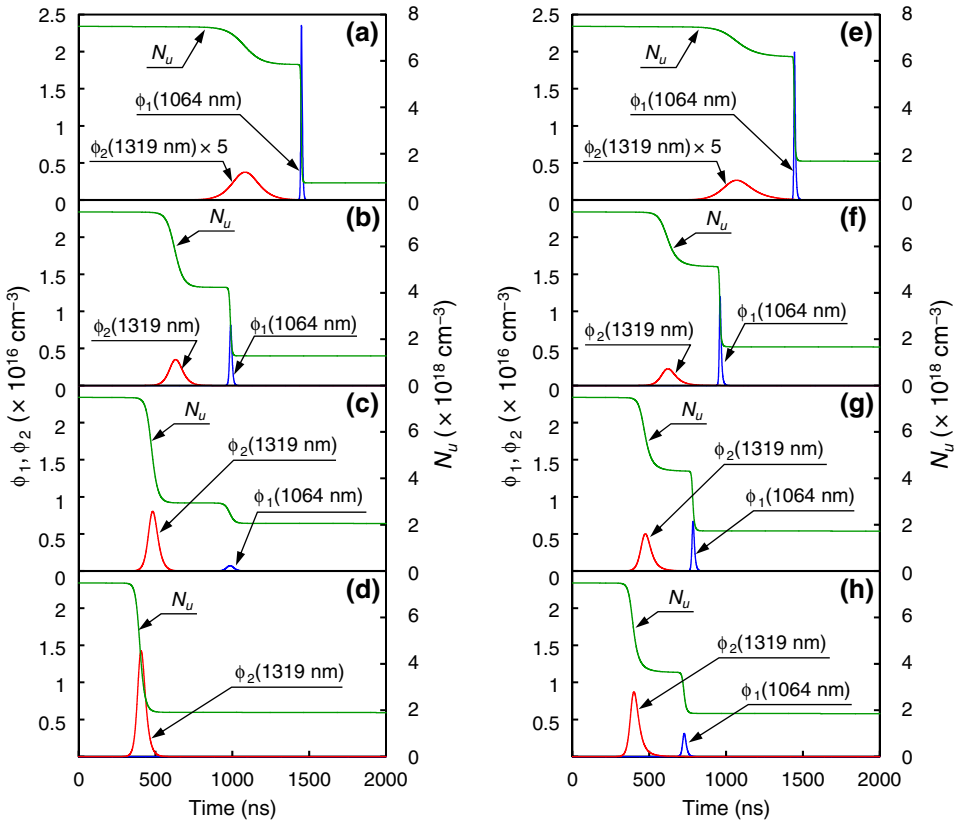

Fig. 3 Results of numerical simulation for dual-wavelength Q-switched operation under two-step energy extraction. *Panels* **a**–**d** $\tau_1 = \tau_2 = 0$ ns; *panels* **e**–**h** $\tau_1 = 11$ ns, $\tau_2 = 80$ ns. Reflectivity of the output mirror for 1064 nm laser is $R_1 = 30$ %. For the 1319 nm laser, reflectivities are as follows: **a** and **e** $R_2 = 55$ %; **b** and **f** $R_2 = 60$ %; **c** and **g** $R_2 = 65$ %; **d** and **h** $R_2 = 70$ %

reflectivity (Fig. 3d, h). The pulse widths of the first pulse in Fig. 3d, h were 59 and 63 ns, respectively. Note that, in these simulations, the second pulse was obtained only by assuming a finite lower-laser-level lifetime, which indicates that the lower-laser-level lifetime is a key design parameter for dual-wavelength Q-switched lasers, in particular, when using the two-step energy extraction. Therefore, understanding the relationship between residual population density and the lower-laser-level lifetime is important for optimizing this laser. Figures 4a, b show, for each laser, the simulation results of the residual population density ($N_{u,f}$ on the vertical axis) of the upper laser level after lasing of the Q-switched pulse. For example, with the two-step energy extraction, residual population $N_{u,f}$ for the 1319 nm laser (Fig. 4b) corresponds to the initial population for the second Q-switched pulse at 1064 nm. The parameters used in this simulation, including the lower-laser-level lifetimes, are the same as for Fig. 3d, h, except for the cavity lengths that were varied from 100 to 3000 mm to change the Q-switched pulse width. The Q-switched pulse width is approximately proportional to the cavity length in all cases. The result for $N_{u,f}$ calculated by the model without the lower-laser-level lifetime (dashed lines) remains almost constant because the energy extraction efficiency is nearly independent of pulse width in our model. However, $N_{u,f}$ increases with decreasing pulse width for the model with the lower-laser-level lifetime (solid curves) because population of the lower laser level due to the laser transition reduces the population inversion, resulting in lower energy extraction efficiency. Even though we used the output mirror with higher reflectivity, the 1319 nm laser tended to have a higher threshold compared with the 1064 nm laser because of the lower stimulated-emission cross section. This means that the 1319-nm transition is suitable for first-pulse generation since the residual population density can be chosen over a relatively wide range. In contrast, the 1064 nm laser has the advantage of a low threshold, resulting in low residual population density and high total-laser efficiency. Therefore, combining the first pulse at 1319 nm and the second pulse at 1064 nm is optimum for dual-wavelength lasers operating with these transitions under the two-step energy extraction.

3 Experimental setup

To confirm the predictions described in the previous section, we developed a diode-pumped Nd:YAG laser using two electro-optic Q-switches, which allowed us to achieve

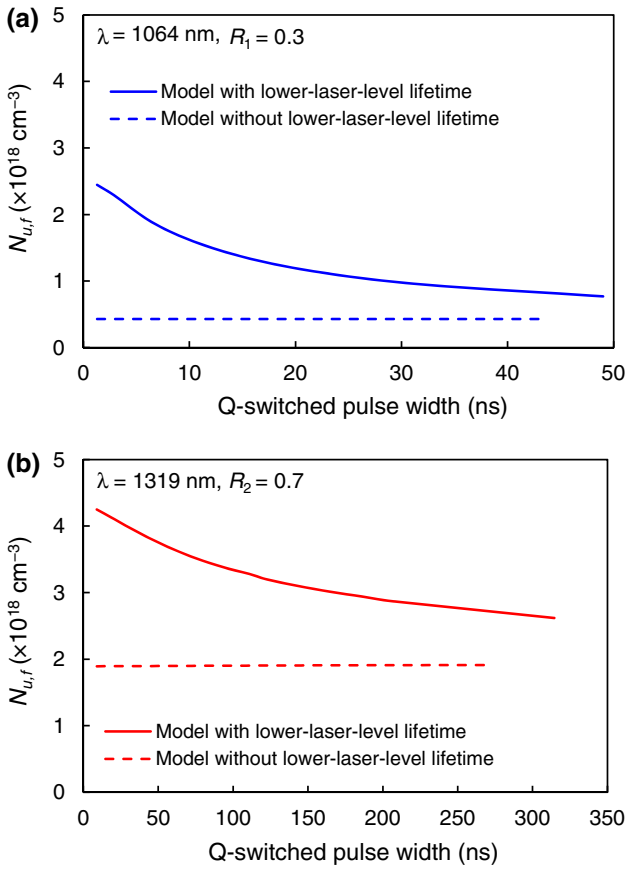

Fig. 4 Calculated residual population densities of upper laser level after Q-switched lasing as a function of Q-switched pulse width. **a** The 1064 nm laser using an output mirror with a 30 % reflectivity. **b** The 1319 nm laser using an output mirror with a 70 % reflectivity

dual-wavelength Q-switched operation using simultaneous and two-step energy extraction because the Q-switch delay times for the two lasers can be independently adjusted to arbitrary temporal positions. Figure 5 shows the cavity configuration of the dual-wavelength Q-switched Nd:YAG laser. The two laser cavities for both wavelengths shared the pump head. For each wavelength, a Q-switch and a rear mirror (M1 or M2) were placed in the respective arm of the cavity. The optical axes of the two arms were separated using two dichroic mirrors (M3 and M4), with high-transmission coating (>99.8 %) at 1064 nm and high-reflection coating (>99.9 %) at 1319 nm. The cavity lengths for the 1064 and 1319 nm lasers were 530 and 650 mm, respectively. This configuration is essentially equivalent to a conventional Y-shaped cavity. The pump head consisted of a laser rod, copper heat sinks, three light guides, and six quasi-CW laser diodes (LDs). Three sets of two LDs were arranged 120° apart around the laser rod. Each LD was capable of delivering 1 kW peak power at a center wavelength of 805 nm. The pump light emitted from the LDs was concentrated by a 50-mm-long light guide and delivered to the lateral surface of the laser rod. The Nd:YAG rod (3 mm in diameter, 15 mm long) was doped with 0.6 % Nd. The end faces of the laser rod were anti-reflection coated at 1064 and 1319 nm. The output mirror M5, used in the dual-wavelength laser experiment with simultaneous energy extraction, was coated with dichroic coating that produced 8 % reflection at 1064 nm and 70 % reflection at 1319 nm. In the two-step energy extraction experiment, M5 was replaced with the output mirror having 30 % reflectivity at 1064 nm, and the output mirror M7 with 55 or 70 % reflectivity at 1319 nm was used because appropriate dichroic output mirrors for this experiment were unavailable. In this case, the two optical axes between the pump head and the output mirrors M5 and M7 were separated by the dichroic mirror M6 coated for high transmission at 1064 nm and high reflection at 1319 nm; however, the cavity lengths remained unchanged. Potassium dideuterium phosphate (KD*P) and beta barium borate (BBO) electro-optic Q-switches were used as the Q-switch elements for 1064 and 1319 nm, respectively. Because Nd:YAG has two closely spaced laser transitions

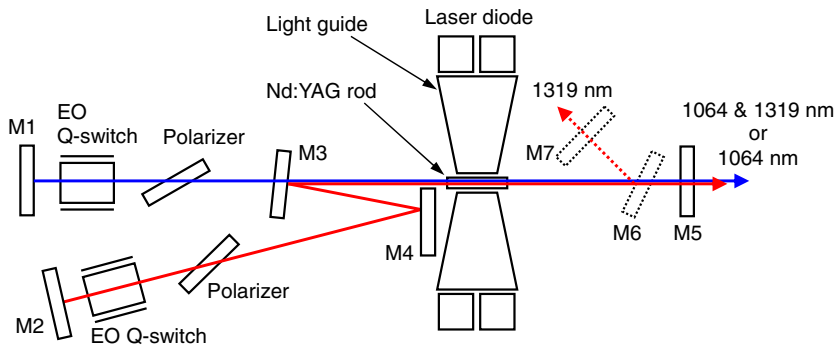

Fig. 5 Cavity configuration of the dual-wavelength Q-switched Nd:YAG laser. M1 and M2, high-reflection mirrors; M3, M4, and M6, dichroic mirrors; M5 and M7, output mirrors. A dichroic output mirror for both the 1064 and 1319 nm lasers was used as M5 in the simultaneous energy extraction experiment. M6 and M7 were only used in the two-step energy extraction experiment, and then M5 and M7 acted as the separated output mirrors for the 1064 and 1319 nm lasers, respectively

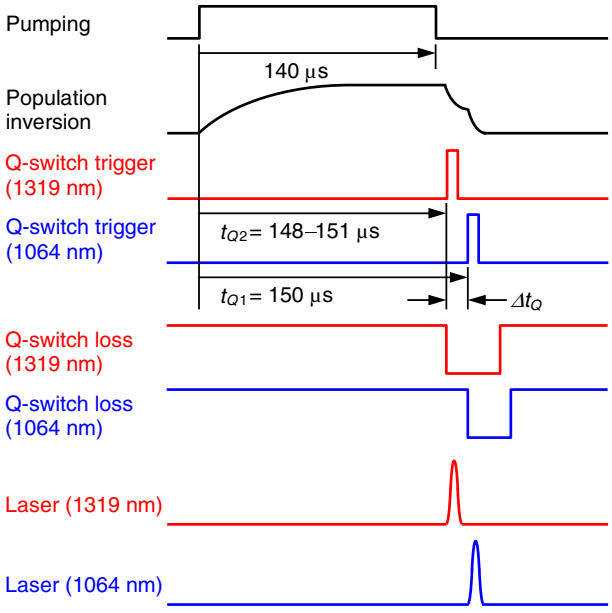

Fig. 6 Timing chart for pump pulse, Q-switch trigger pulses, Q-switch losses, and Q-switched laser pulses

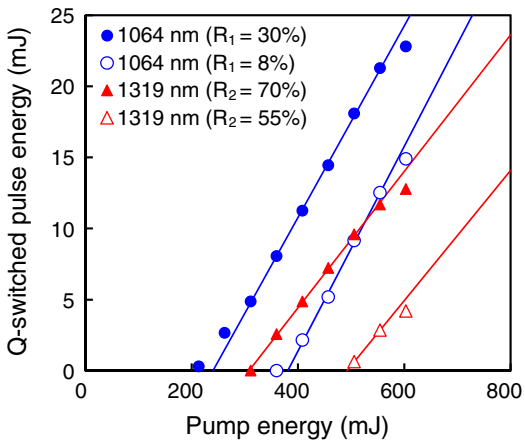

Fig. 7 Q-switched pulse energies of Nd:YAG laser operating at each single emission line as a function of pump energy

(1319 and 1338 nm), the rear mirror M2 for the 1319 nm laser had a high-transmission coating for 1338 nm in addition to a high-reflection coating for 1319 nm.

Figure 6 shows a timing chart of our dual-wavelength laser experiments in Q-switched mode. The pump and two Q-switch trigger pulses were generated using a digital delay generator (Stanford Research Systems, Inc., DG535). The nominal timing jitter of this pulse generator was less than 100 ps. In our laser system, amplified spontaneous emission occurred at higher pumping levels. To avoid amplified spontaneous emission, pump energy was limited to approximately 600 mJ, which is lower than the available maximum pump energy. This allowed us to choose the appropriate combination of pump power and pump pulse length. The pump LDs were derated to 4307 W total peak power, which corresponds to approximately 70 % of the maximum available power at drive current of 75 A to mitigate the shortening of their operational lifetime. Accordingly, the pump pulse length was set to 140 μs. Whereas this pulse length was 1.6 times shorter than the upper laser manifold lifetime of 230 μs, the energy storage efficiency is expected to be 1.2 times higher for the 140 μs pulse than for the 230 μs pulse. The Q-switch for the 1064 nm laser was opened 150 μs after initiation of the pump pulse. The Q-switch trigger time for the 1319 nm laser was adjusted between 148 and 151 μs. Q-switched pulses at 1064 and 1319 nm were simultaneously monitored with Si and InGaAs photodiodes, respectively, connected to a 350 MHz digital oscilloscope (Instek GDS-3354).

4 Experimental results and discussion

4.1 Single-emission-line operation

Laser experiments were performed at a pulse repetition frequency of 10 Hz. Although the pump LDs could produce a total pump energy of 1.2 J, the laser was operated with a total pump energy of 603 mJ, which corresponds to a total pump power of 4307 W and a pump pulse length of 140 μs. Figure 7 shows the Q-switched pulse energies of the two lasers operating at a single emission line as a function of pump energy for different output mirrors. The curves are least-square fits to the experimental data. A maximum pulse energy of 22.8 mJ was obtained with the output mirror with 30 % reflectivity at 1064 nm; the pulse width for this configuration was 16 ns. In contrast, the 1319 nm laser led to a higher threshold compared with the 1064 nm laser, even when the output mirror with 70 % reflectivity was used. The pulse energies for output mirrors with 55 and 70 % reflectivities were 4.2 and 12.8 mJ, respectively. Because of the small stimulated-emission cross section, pulse widths for the 1319 nm laser were longer than 70 ns, even at the highest pumping level. The characteristics of the output of the 1064 nm laser with the output mirror with 8 % reflectivity were similar to those of the 1319 nm laser with the output mirror with 70 % reflectivity, albeit with slight differences in slope efficiency and threshold. When we used the output mirrors with 30 % reflectivity for the 1064 nm laser and 70 % for the 1319 nm laser, the root mean square (RMS) fluctuations in the pulse energies for the 1064 and 1319 nm lasers were 1.5 and 4.7 %, respectively; these values correspond to the minimum achievable fluctuations in dual-wavelength operation.

4.2 Dual-wavelength operation

The combination of output mirror reflectivities of 8 and 70 % at 1064 and 1319 nm, respectively, was suitable to obtain the same output level for simultaneous dual-wavelength operation. In dual-wavelength lasing with the two-step energy extraction process, the total efficiency of the dual-wavelength laser depends on the performance of the laser that generated the second pulse. Therefore, the 1064 nm laser, with the output mirror with 30 % reflectivity, was preferred for second pulse lasing in our system. In this case, we expected to achieve two-step energy extraction for both the output mirrors of the 1319 nm laser.

The laser experiment with simultaneous energy extraction was performed using the output mirror with 8 and 70 % reflectivities at 1064 and 1319 nm, respectively. Figure 8a shows the Q-switched pulse energies for two wavelengths as a function of the time interval between the two Q-switch trigger times Δt_Q. Each experimental datum represents the average of 30 shots. The solid and dashed curves correspond to the calculated results with and without the effects of the lower-laser-level lifetimes, respectively. Despite the 1319 nm laser having a later Q-switch delay time compared with that of the 1064 nm laser, lasing occurred only at 1319 nm when $\Delta t_Q > -90$ ns. One possible reason for this discrepancy is that the electrical signal delay inside the Q-switch driver differs between the two lasers. When we monitored the Q-switch trigger pulses and the high-voltage signals of the two lasers, we found that under the same trigger timing, onset of the high voltage applied to the Q-switch device for the 1064 nm laser occurred several hundred nanoseconds after that for the 1319 nm laser. This makes for a Q-switch opening time between the two lasers that is long compared with Δt_Q. However, the difference between the two lasers in buildup time of the Q-switched pulse also contributes to the discrepancy between the Q-switch trigger interval and the laser-pulse interval. The stimulated-emission cross section for the 1319-nm transition is approximately five times smaller than that for the 1064-nm transition. Therefore, if we require a threshold energy comparable with that of the 1064 nm laser, the output coupling of the 1319 nm laser must be five times smaller than that of the 1064 nm laser (under the assumption of negligible roundtrip loss). In other words, to reach threshold with the same population density in the upper laser level, the 1319 nm laser requires more intracavity roundtrips than the 1064 nm laser. This requirement leads to a long buildup time for the Q-switched pulse, thereby producing an additional temporal delay for the 1319 nm laser pulse. As a result of these two opposing effects, Δt_Q differs from the time interval between the two Q-switched pulses in our system.

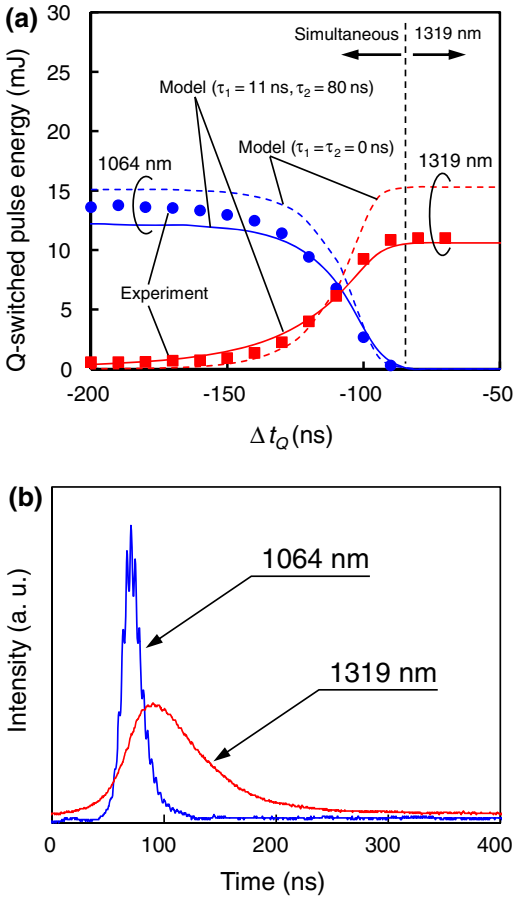

Fig. 8 **a** Observed and calculated pulse energies for dual-wavelength laser under simultaneous energy extraction as a function of time between two Q-switch delay times Δt_Q. **b** Typical pulse shapes for $\Delta t_Q = -106$ ns

Furthermore, an error arising from the estimate of the initial photon densities, which cannot be exactly determined, was also included in the calculations. Accordingly, with respect to the experimental data, all calculated Δt_Q were shifted by approximately -325 ns to fit. This shift is reasonable because the calculated pulse energy does not depend on the initial photon density. Dual-wavelength lasing was achieved for $\Delta t_Q < -90$ ns. The output energy of the 1064 nm laser decreased with increasing Δt_Q, as expected from the numerical simulation (Fig. 2). Two Q-switched pulses were simultaneously generated during dual-wavelength operation, although partial temporal overlap between the two pulses was obtained because of the difference in pulse width. When operating the laser at $\Delta t_Q = -106$ ns, the pulse energies for the two wavelengths became comparable. In this case, Q-switched pulse energies of 6.8 and 6.1 mJ with pulse widths of 17 and 73 ns were obtained at 1064 and 1319 nm, respectively (Fig. 8b). The RMS fluctuations at both wavelengths exceeded 14 % because of line competition between the

two laser transitions. Under same conditions, the calculated pulse widths of the 1064 and 1319 nm lasers were 16–18 and 55–61 ns, respectively. Although the pulse width of the 1319 nm laser was longer than that predicted by the model, the agreement was still sufficient to compare the two models. The model including the effect of the lower-laser-level lifetime was consistent with the experimental results, but the total energy of the two Q-switched pulses calculated without the effect of the lower-laser-level lifetime was somewhat higher than the experimental data when the 1319 nm laser transition was dominant. In simultaneous dual-wavelength lasing, the ratio of the pulse energies can be arbitrarily chosen by adjusting the time interval between the Q-switch trigger pulses. Consequently, the lower-laser-level lifetimes mainly affect the total energy of the two Q-switched pulses when they are comparable to or longer than the Q-switched pulse width.

Unlike the simultaneous dual-wavelength lasing technique, very stable output energy can be expected for the two-step energy extraction lasing technique. For this experiment, we used the output mirror with a 30 % reflectivity for the 1064 nm laser and 55 % reflectivity for the 1319 nm laser. The threshold pump energy for the 1319 nm laser was approximately 2.5 times higher than that for the 1064 nm laser (Fig. 7). Figure 9a, b show the calculated and observed pulse energies for the dual-wavelength Q-switched laser and the observed pulse shapes for $\Delta t_Q = 1300$ ns, respectively. In this condition, an output energy of 4.2 mJ was extracted at 1319 nm, which is equivalent to that for single-emission-line operation. Following this, an output energy of 17.7 mJ was obtained for the second pulse at 1064 nm. The sum of both pulse energies was 21.9 mJ, which agrees with the pulse energy of the 1064 nm laser under single-emission-line operation, if the difference in quantum defects between the two lasing wavelengths is accounted for. This result indicates that the residual energy in the upper laser manifold, after extracting the first pulse, can be extracted efficiently for the second pulse. The time interval between the two Q-switched pulses decreased with decreasing Δt_Q, and the change in the laser pulse interval was approximately equivalent to the change in Δt_Q. For $\Delta t_Q < 1000$ ns, temporal overlap occurred between the two pulses. When the laser operated without temporal overlap between the two pulses, high stability, comparable to that in single-emission-line operations, was achieved by avoiding line competition for any pulse timing. As a result, RMS fluctuations of 1.5 and 4.8 % were achieved with 1064 and 1319 nm lasers, respectively. Since the ratio of the two pulse energies strongly depends on the energy extracted as a first pulse for this lasing method, the relationship between the pulse width of 1319 nm laser and the lower-laser-level lifetime is particularly important. The pulse width of 1319 nm laser was

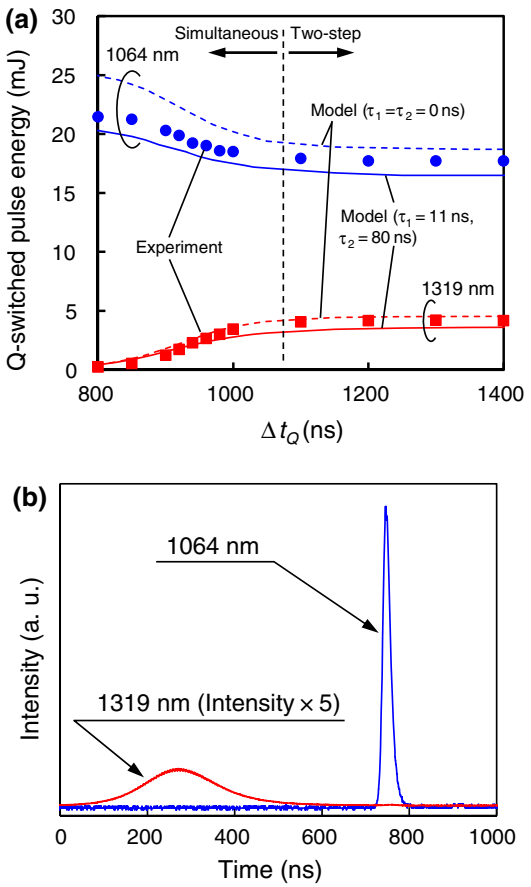

Fig. 9 **a** Observed and calculated pulse energies of dual-wavelength laser under two-step energy extraction as a function of time interval between two Q-switch delay times Δt_Q. The reflectivities of the output mirror at 1064 and 1319 nm were 30 and 55 %, respectively. **b** Typical pulse shapes for $\Delta t_Q = 1300$ ns

measured to be 197 ns, which is slightly shorter than the calculated pulse width of 222 ns. However, these values are more than two times longer than the assumed lower-laser-level lifetime, which means that both models yielded similar results and were consistent with the experimental results. Because the observed pulse width for 1064 nm laser was 21 ns, which is two times longer than the calculated value, the effect of the lower-laser-level lifetime was slightly reduced in comparison with the model. Unlike the simultaneous energy extraction shown in Fig. 8, ratio of the two pulse energies for two-step energy extraction can be tuned by changing the threshold pump energies and/or the maximum output energies in single-emission-line operation.

We also demonstrated dual-wavelength lasing for the other combination of output mirror reflectivities. Figure 10a shows the Q-switched pulse energies as a function of Δt_Q for the dual-wavelength laser with the output mirror with 30 % reflectivity for the 1064 nm laser and 70 % reflectivity for the 1319 nm laser. The other conditions

were the same as for Fig. 9. Figure 10b shows the typical pulse shapes for $\Delta t_Q = 140$ ns. Because of the lower output coupling for the 1319 nm laser, threshold pump energy for this wavelength reduced from 492 to 311 mJ, and the maximum output energy thereby increased from 4.2 to 12.8 mJ, as shown in Fig. 7. For $\Delta t_Q > 110$ ns, two-step energy extraction was achieved, and the laser produced an output energy of 12.6 mJ in the first pulse at 1319 nm and 6.7 mJ in the second pulse at 1064 nm. Root mean square fluctuations of 4.7 and 2.6 % were observed for the 1319 and 1064 nm lasers, respectively. In comparison with the experimental results shown in Fig. 9, pulse width of the 1064 nm laser increased from 21 to 44 ns, while that of the 1319 nm laser decreased from 197 to 96 ns. Therefore, time interval between the peak positions of the two pulses decreased from 505 to 245 ns. If shorter pulse widths were achieved, then shorter time intervals should be possible. For example, a dual-wavelength laser operating with pulse widths of the order of a few nanoseconds or shorter allowed us to achieve temporal overlap between the two pulses using a delay line for the first pulse. The calculated pulse widths of the 1319 nm laser for both models were 60–64 ns, which are approximately 1.6 times shorter than those observed experimentally. According to the numerical simulation shown in Fig. 4b, the ratio of residual population density of the upper laser level (in the model that accounts for the lower-laser-level lifetime) to that in the model assuming negligible lifetime is 1.8 and 1.9 for pulse widths of 96 and 60 ns, respectively. Thus, even in our experiment, the energy extraction is characterized by the finite lower-laser-level lifetime. The calculated results that include the effect of the lower-laser-level lifetime agreed reasonably well with the experimental results. In addition, all numerical simulations were performed assuming $\tau_1 = 115$ ps [20] to ensure that the $^4I_{11/2}$ manifold lifetime used in our simulations ($\tau_1 = 11$ ns) was reasonable. Because such a subnanosecond lifetime was significantly shorter than the Q-switched pulse widths of the 1064 nm laser presented in this study, the calculated results were the same as those assuming $\tau_1 = 0$ ns and $\tau_2 = 80$ ns. This led to the overestimations of the 1064 nm pulse energies. Note that another model would not predict the second pulse energy due to the small residual population density of the upper laser level after lasing of the first pulse, which indicates that the lower-laser-level lifetime affects not only the total energy of the two Q-switched pulses but also the ratio of the two pulse energies in the case of two-step energy extraction. Consequently, compared with simultaneous energy extraction, designing a dual-wavelength laser using the two-step energy extraction technique requires a detailed model.

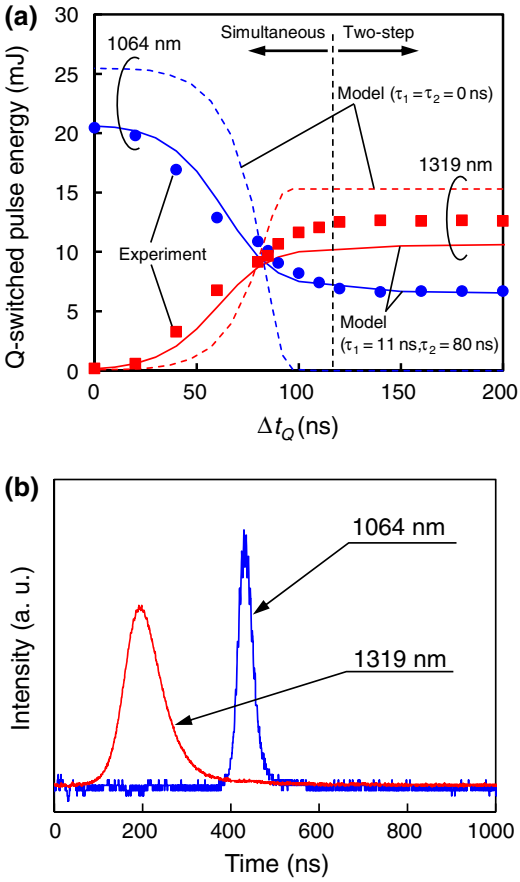

Fig. 10 **a** Observed and calculated pulse energies for dual-wavelength laser under two-step energy extraction as a function of time interval between two Q-switch delay times Δt_Q. The reflectivities of the output mirror at 1064 and 1319 nm were 30 and 70 %, respectively. **b** Typical pulse shapes for $\Delta t_Q = 140$ ns

5 Conclusion

We have investigated the effects of lower-laser-level lifetimes on extracted energies in dual-wavelength Q-switched lasers with a common upper laser level. Numerical simulations of the temporal behavior of dual-wavelength Q-switched pulses and population density of the upper laser level were performed using a rate-equation model and accounting for the lifetime of finite lower laser manifold. Because of the reduced residual population density of the upper laser level after lasing when the Q-switched pulse width is comparable to or shorter than the lower-laser-level lifetime, higher extracted energies were calculated using the model without the effect of the lower-laser-level lifetime than using the model with this effect. To confirm the predictions of the model, a dual-wavelength Q-switched Nd:YAG laser operating at 1064 and 1319 nm was implemented via the simultaneous and two-step energy

extraction techniques. Two Q-switched pulses with an energy of the order of 20 mJ were obtained with pulse widths comparable to or shorter than the lower-laser-level lifetimes. Provided the effect of the lower-laser-level lifetime was considered, predictions of the model agreed reasonably well with the experimental results. In addition, a comparison of the experimental and calculated results indicated that the lower-laser-level lifetime affected not only the total energy of the two Q-switched pulses but also the ratio of the two pulse energies for two-step energy extraction, whereas the lower-laser-level lifetime affected only the total energy for simultaneous energy extraction. We found that the effects of the lower-laser-level lifetimes should be considered to build an accurate model for designing dual-wavelength lasers that use two-step energy extraction.

References

1. N.P. Barnes, B.M. Walsh, in *Advanced Solid-State Photonics (TOPS)*, vol. 94 of OSA trends in optics and photonics (Optical Society of America, 2004), paper 269
2. B.M. Walsh, Laser Phys. **20**, 622 (2010)
3. A. Saha, A. Ray, S. Mukhopadhyay, N. Sinha, P.K. Datta, P.K. Dutta, Opt. Express **14**, 4721 (2006)
4. K. Asai, A. Sato, T. Terasaki, N. Sugimoto, Proc. SPIE **7860**, 78600G-1 (2010)
5. W. Lin, H. Shen, J. Appl. Phys. **86**, 2979 (1999)
6. Y. Chen, S.W. Tsai, Opt. Lett. **27**, 397 (2002)
7. J.L. He, J. Du, J. Sun, S. Liu, Y.X. Fan, H.T. Wang, L.H. Zhang, Y. Hang, Appl. Phys. B **79**, 301 (2004)
8. H.Y. Shen, W.X. Lin, R.R. Zeng, Y.P. Zhou, G.F. Yu, C.H. Huang, Z.D. Zeng, W.J. Zhang, R.F. Wu, Q.J. Ye, Appl. Opt. **32**, 5952 (1993)
9. R.W. Farley, P.D. Dao, Appl. Opt. **34**, 4269 (1995)
10. H.X. Li, Y.X. Fan, P. Xu, S.N. Zhu, P. Lu, Z.D. Gao, H.T. Wang, Y.Y. Zhu, N.B. Ming, J. Appl. Phys. **96**, 7756 (2004)
11. X.W. Fan, J.L. He, H.T. Huang, L. Xue, IEEE J. Quantum Electron. **43**, 884 (2007)
12. H.T. Huang, J.L. He, B.T. Zhang, K.J. Yang, C.H. Zuo, J.L. Xu, X.L. Dong, S. Zhao, Appl. Phys. B **96**, 815 (2009)
13. J.L. Xu, H.T. Huang, J.L. He, J.F. Yang, B.T. Zhang, X.Q. Yang, F.Q. Liu, Appl. Phys. B **103**, 75 (2011)
14. J.J. Degnan, D.B. Coyle, R.B. Kay, IEEE J. Quantum Electron. **34**, 887 (1998)
15. T.Y. Fan, IEEE J. Quantum Electron. **24**, 2345 (1988)
16. H. Su, H.Y. Shen, W.X. Lin, R.R. Zeng, C.H. Huang, G. Zhang, J. Appl. Phys. **84**, 6519 (1998)
17. W. Lin, S. Lin, J. Huang, J. Opt. Soc. Am. B **20**, 479 (2003)
18. G.A. Henderson, J. Appl. Phys. **68**, 5451 (1990)
19. F.E. Hovis, M. Stuff, C.J. Kennedy, B. Vivian, IEEE J. Quantum Electron. **28**, 39 (1992)
20. C. Bibeau, S.A. Payne, H.T. Powell, J. Opt. Soc. Am. B **12**, 1981 (1995)
21. S.P. Ng, D.Y. Tang, L.J. Qian, L.J. Qin, IEEE J. Quantum Electron. **42**, 625 (2006)
22. S. Singh, R.G. Smith, L.G.V. Uitert, Phys. Rev. B **10**, 2566 (1974)
23. D. Hua, Z. Song, S. Wang, Z. Rong, J. Chem. Phys. **89**, 5398 (1988)